

Aerosol Measurement in the Australian Outback: Intercomparison of Sun Photometers

R. M. MITCHELL

CSIRO Atmospheric Research, Earth Observation Centre, Canberra, Australia

B. W. FORGAN

Bureau of Meteorology, Melbourne, Australia

(Manuscript received 3 January 2002, in final form 8 May 2002)

ABSTRACT

The low background aerosol loadings prevailing over much of the Australian continent necessitate careful attention to the calibration of sun photometers. The validity of such calibrations can only be assessed objectively by intercomparison of independent systems operating side by side. This paper documents two intercomparisons: the first between three dissimilar photometers collocated at Alice Springs using independent calibration methods, and the second between identical photometers sited at Tinga Tingana in the Strzelecki Desert of South Australia.

The intercomparison of total optical depth derived from two Cimel CE318 systems at Tinga Tingana shows negligible biases (<0.0004) at all four wavelengths. Instantaneous differences in total optical depth are used to infer 95% uncertainty intervals, which range from 0.003 at 670 nm to 0.005 at 870 nm. The Alice Springs intercomparison shows negligible bias between the Carter–Scott SPO1A and Cimel CE318 at 500 nm, while a bias of 0.004 between the two at 868 nm is identified as sideband leakage in one of the filters. The 95% uncertainty interval for each instrument is <0.007 at both 500 and 868 nm. The multifilter rotating shadowband radiometer (MFRSR) shows a consistent positive bias of 0.012–0.014 at the three wavelengths studied, most probably related to issues of alignment and angular response characterization. The 95% uncertainty interval is greater than 0.02, comparable with the typical background midvisible aerosol optical depth at these sites. Hence this instrument is unsuitable for the measurement of background aerosol under Australian conditions without careful characterization.

The impact of uncertainties in surface pressure and ozone on aerosol optical depth is shown to be negligible for the case where the surface pressure is measured on site, and the ozone amount is taken from monthly mean data from stations of commensurate latitude to the observing site. Comparison with previous work suggests that calibration of collimated sun photometers at remote inland sea level Australian sites yields accuracy exceeding that obtained from techniques presently in use in the Northern Hemisphere involving calibration at high altitude sites.

1. Introduction

The role of aerosol in moderating climate change is now well recognized (Penner et al. 2001), both through the scattering and absorption of incoming solar radiation by aerosol (the so-called direct effect) and via the modification of cloud droplet size, leading to changed cloud-top reflectance and cloud lifetime (the indirect effect; e.g., Rotstain 1999). However, much uncertainty remains as to the magnitude of these effects, stemming largely from the lack of a comprehensive knowledge of regional and seasonal differences in aerosol properties across the globe.

Considerable progress in this area has been made in recent years by large field campaigns directed at elucidating the properties of specific aerosol regimes. For example, the Aerosol Characterization Experiment (ACE) series has focused successively on the aerosols

of the pristine Southern Ocean (ACE-1), and pollution and dust aerosol over the Northern Atlantic Ocean (ACE-2), while the recent ACE-Asia mission studied dust aerosol emanating from northern Asia. The TARFOX mission focused on anthropogenic aerosol off the east coast of the United States (Russell et al. 1999). Smoke aerosol originating from biomass burning has been subject to many field experiments including several over the Amazon basin (BASE-A, Kaufman et al. 1992; BASE-B, Ward et al. 1992; SCAR-B, Christopher et al. 2000) and southeast Asia (Gras et al. 1999).

While these field campaigns are important in establishing the physical and chemical properties of aerosol in a variety of regimes, knowledge of global distribution and seasonality requires a long-term measurement strategy. This requirement has led to the deployment of sun photometer networks such as that associated with the Atmospheric Radiation Measurement program (ARM; Michalsky et al. 2001) and the Aerosol Robotic Network (AERONET) initiative (Holben et al. 1998, 2001). AERONET consists of a worldwide network of over 100 sun photometers coordinated through the National

Corresponding author address: Dr. Ross M. Mitchell, CSIRO Earth Observation Centre, P.O. Box 3023, Canberra, ACT 2601, Australia.
E-mail: Ross.Mitchell@csiro.au

Aeronautics and Space Administration's (NASA) Goddard Space Flight Center, with affiliations to contributing subnetworks on all continents.

To date little attention has been focused on the characterization of Australian continental aerosol, even though Australia is a significant source of smoke aerosol from seasonal biomass burning in the tropical north (Scott et al. 1992). In addition, the Australian deserts are well known as sources of wind-blown dust (McTainsh and Pitblado 1987), and they constitute a substantial aerosol source in simulations of the impact of dust on climate (Tegen and Fung 1994; Tegen et al. 1996). Furthermore, it is now clear that Australia is the recipient of long-range transport of aerosol from southern Africa and even South America (Rosen et al. 2000).

In order to address the comparative lack of understanding of Australian continental aerosol, a two-pronged strategy is being pursued, consisting of a combination of surface measurements and satellite retrievals. The surface measurements are based on independent but complementary instrumental networks operated by the Australian Bureau of Meteorology (BoM) and the Commonwealth Scientific and Industrial Research Organisation (CSIRO). The BoM instruments, as part of its radiation network, are located at meteorological observing stations, and are configured to the majority of Baseline Surface Radiation Network protocols; the network places a priority on the impact of extinction components on the surface radiation budget. The CSIRO Aerosol Ground Station Network (AGSNet) was established with a view toward the characterization of specific aerosol types, in particular smoke from biomass burning and wind-blown dust, to promote the validation of satellite aerosol retrievals through the selection of sites with uniform surface properties, and to provide data to facilitate atmospheric correction of satellite images. In addition, AGSNet was instrumented with sun photometers compatible with AERONET, to facilitate data distribution through that network.

The BoM Alice Springs station is Australia's contribution to the World Climate Research Programme (WCRP) Baseline Surface Radiation Network (BSRN; Ohmura et al. 1998) and its schedule of measurements and operational principles are closely aligned with the BSRN measurement philosophy. Recently a BSRN working group established a preliminary protocol to provide spectral irradiance and optical depth data to the global community using a systematic data protocol (WMO 2001). The BSRN study showed that, provided modern automatic instruments and good calibration procedures were used, analysis with a uniform algorithm could produce 95% uncertainties in aerosol optical depth of less than 0.010. However, as there are a plethora of different algorithms and extinction models, and as yet poor estimates of solar spectral irradiance, the resulting protocol will establish a direct spectral transmission archive. The spectral components of the BoM radiation program conform to this preliminary protocol and thus

eliminate a significant number of problems cited in the Background Air Pollution Monitoring Network (BAPMoN) turbidity archive (Forgan et al. 1994).

As a preliminary step toward the assembly and dissemination of datasets from both Bureau of Meteorology and CSIRO networks, it is important to establish benchmark accuracies for the systems in measuring aerosol optical depth under Australian conditions. Existing unpublished data for midvisible aerosol optical depths from Australian inland stations show a seasonal cycle peaking around 0.08 in early spring (September), and a minimum of ~ 0.02 extending through late autumn and winter. Since these levels are substantially lower than those usually encountered in the Northern Hemisphere, measurement accuracies must be correspondingly higher to maintain comparable relative error. This paper reports the result of two intercomparison experiments, the first between three different sun photometers located at the Bureau of Meteorology observing station at Alice Springs over the period February–May 2000. The differences between the systems include not only hardware, but calibration strategy as well, so that the results provide a useful benchmark for accuracies achievable by essentially independent systems. The second intercomparison was between identical Cimel instruments located at CSIRO's Tinga Tingana site in the Strzelecki Desert of South Australia. Since both hardware and processing software were identical in this case, this comparison provides a measure of instrumental precision obtainable from the Cimel instrument under Australian conditions.

2. Description of systems

a. Bureau of Meteorology spectral transmission program

Figure 1 shows the location of the BoM radiation stations and the CSIRO's AGSNet sites. Each BoM site is monitoring spectral direct irradiance components in at least five spectral bands (typically 412, 500, 610, 778, and 862 nm) with a 1-min sampling rate. Alice Springs in central Australia is one of these sites, being one of three special sites (the others being Cape Grim and Melbourne) that also incorporate solar aureole measurements using Carter–Scott Design SPO1A radiometers. Given the relative high uncertainty in solar spectral irradiance standards the processed data are stored in the form of transmissions. The SPO1A-type measurements commenced operation at Cape Grim in 1997, Alice Springs in 1996, and Melbourne in 1998; there have been measurements at Cape Grim using a SPO1-type instrument since 1984. The 12 other BoM sites use one or two Carter–Scott SPO2 radiometers that have gradually been brought online since 1997.

1) SPO1A RADIOMETER

The direct solar spectral irradiance signals at Alice Springs were measured with an SPO1A radiometer. The

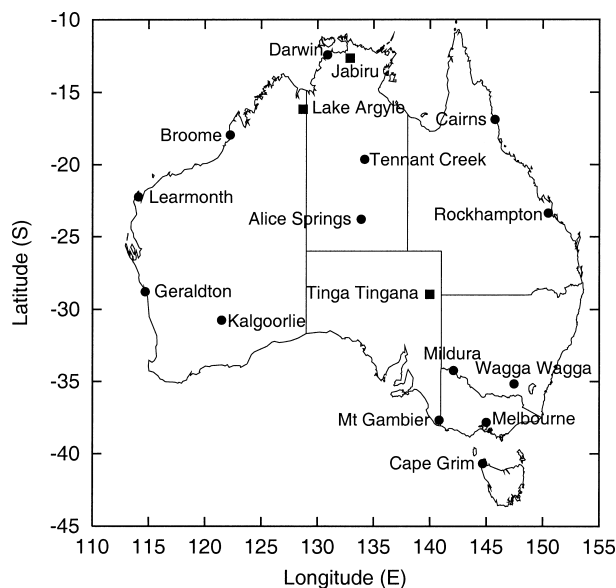


FIG. 1. Location of observation sites across the Australian continent. BoM radiation measurement sites are shown as filled circles, while CSIRO aerosol ground stations are shown as filled squares.

instrument, serial number 1001, consists of four independent spectral radiometers and an aperture wheel with three positions: closed, direct beam, and aureole. In a single measurement cycle, each radiometer provides four measurements based on the three possible aperture positions. Two radiometers provide closed, direct beam, aureole, and closed data, while the remaining two provide closed, aureole, direct, and closed data. The duplication of the closed position provides zero irradiance readings before and after each pair of signal readings. In direct beam position the full field of view is 2.4° with slope angle 0.8° . In the aureole position the field of view approximates an annulus enclosed between view angles 3° and 5° centered on the sun. Stray light is minimized via baffles that prevent direct solar irradiance illuminating the limiting apertures. For the work reported below, the aureole measurements from the SPO1A were not used.

The measurement cycle described above ensures that each filter is only exposed to direct solar irradiance for approximately 2 s each minute. The filters were 25-mm-diameter interference filters with full width at half maximum (FWHM) of 5 nm, and peak transmission at approximately 368, 500, 610, and 868 nm. The four radiometers are mounted in a temperature-stabilized housing maintained at 40°C . The SPO1A is mounted on one of a pair of active altitude-azimuth solar tracking systems with a pointing uncertainty of 0.03° in direct sun conditions. The active sensor (Sibson and Forgan 1987), a pinhole quadrant silicon detector, is also filtered at 868 nm (10 nm FWHM) and its total signal is closely equivalent to a direct radiometer with a field of view of 14° .

2) MFRSR

In addition to the SPO1A, a multifilter rotating shadowband radiometer (MFRSR) was on site at Alice Springs. The instrument was deployed by N. Larsen of Pacific Northwest National Laboratory. The instrument recorded spectral global and diffuse irradiance signals at 1-min intervals in bands of approximately 12 nm FWHM at wavelengths 412, 550, 610, 675, 778, 868 nm, when the sun was above the horizon. The instrument type is well described by Harrison et al. (1994). The angular response of the instrument was calibrated by the manufacturer immediately prior to installation at Alice Springs. Leveling was performed using a procedure devised to optimize the horizontal alignment of the sensor element regardless of the positioning of the instrument housing.

3) DATA COLLECTION

The voltage signals from the SPO1A and active sensor peaked in the range of 1–5 V during clear sun conditions and were monitored by a 16-bit data system with a signal resolution of 1 mV for signals >50 mV and $10 \mu\text{V}$ for signals ≤ 50 mV. The data system integrated the voltage signals over five power line cycles (at 50 Hz) to reduce noise. Examination of the zero irradiance signals indicates that the precision of the reported direct sun signals was better than 1 mV.

A measurement cycle for the SPO1A consisted of a zero irradiance measurement from each detector, an aperture movement to expose two channels to direct irradiance and the other two to aureole irradiance, measurements from each detector, an aperture movement to reverse the measurement type, measurements from each detector, and a final aperture movement to the zero irradiance position and subsequent measurement. The entire cycle lasts 9 s with 4 s separating direct irradiance measurements in all channels. When the MFRSR was on site, the mean time of the direct measurements was at approximately 7 s after the minute; this coincided with the diffuse irradiance measurement of the MFRSR.

As part of the standard solar tracking quality assurance protocol of the sites, the total signal from the active sensor was sampled at 1 Hz and the standard deviation for the previous minute and the sample at 7 s past the minute were stored. All Australian sites involved in the BoM radiation network are radiosonde meteorological stations that are staffed daily, with minute data recorded for atmospheric pressure, temperatures, wind speed and direction, and rainfall. All irradiance and surface meteorological measurements were recorded in Australian central standard time (UTC + 9.5 h) and maintained to within ± 1 s of the true time by use of Internet time standards. Data were downloaded to the BoM central radiation network archive the morning of the following day via the Internet.

MFRSR data were downloaded daily prior to the fol-

lowing sunrise using standard MFRSR protocols via a telephone modem connection. Time maintenance was done remotely to keep within ± 5 s (N. Larsen 2001, personal communication).

b. CSIRO AGSNet

The AGSNet system was developed to carry out aerosol measurement at remote locations. Its instrument complement includes a CE318 Cimel sun/sky photometer, an M903 Radiance Research nephelometer, and environmental sensors recording barometric pressure, temperature, relative humidity, and wind speed and direction. In its remote configuration the system is powered by a solar panel charging a storage battery, and data are transferred via a commercially available satellite telephone. Currently operational stations are located at Tinga Tingana in the Strzelecki Desert in central Australia, Lake Argyle in the Kimberly region of Western Australia, and Jabiru in the Northern Territory. For the installation at Alice Springs, a simplified version of the system was built to support just the sun photometer and barometer. Mains power was available and data were collected on the BoM radiation station computer and downloaded to the central facility every morning.

CE318 SUN/SKY PHOTOMETER

This instrument has been described at length by Holben et al. (1998) so only a brief outline is given here. The photometer consists of a sensor head mounted on a two-axis robotic sun tracking system. Acquisition is achieved by pointing to the computed solar position, then locking onto the solar disk using a four-quadrant detector. The sensor head contains dual entrance apertures for the direct sun and sky scanning measurements; external collimators are affixed to these to provide stray light rejection. The field of view of both sensors is 1.2° . An eight-position rotating filter wheel provides spectral channel selection for both sun and sky silicon photodiode detectors. For the instrument deployed at Alice Springs (no. 4) the spectral channel effective wavelengths and half-power bandpasses in nanometers were 380(5), 440(10), 500(5), 670(10), 778(5), 870(10), 936(10), and 1020(10). The corresponding configuration of the two instruments at Tinga Tingana (nos. 2 and 3) was 440(10), 670(10), 870(10), 936(10), and 1020(10). The 936-nm channel is intended for the retrieval of water vapor loading. The temperature of the detectors is measured to allow compensation, in practice only necessary for the 1020-nm channel.

The predefined observation regime involves direct sun measurements based on fixed airmass increments of 0.5 and 0.25 over the ranges 7–5 and 5–2, respectively. For an air mass less than 2, solar acquisition takes place every 15 min.

c. Sun photometer calibration

1) SPO1A AND MFRSR

A primary effort in establishing spectral radiometer networks is to determine the extinction components, particularly aerosol optical depth, by application of the Lambert–Beer–Bouguer law. Aerosol optical depth is the measure of extinction by aerosols (or suspended particulate matter) in the vertical atmospheric column and is a quantity derived from values of transmission in spectral bands where the primary components of extinction are molecular (τ_m), aerosol (τ_a), and ozone extinction (τ_o). Deriving τ_a is in principle a simple exercise using the Lambert–Beer–Bouguer law as applied to direct sun observations in the atmosphere, namely:

$$S(t, \lambda, m) = S_0(\lambda)D(t)^{-2} \exp(-\tau_m m_m - \tau_a m_a - \tau_o m_o), \quad (1)$$

or transformed into natural logarithms as

$$\ln S(t, \lambda, m) = \ln S_0(\lambda) - 2 \ln D(t) - \tau_m m_m - \tau_a m_a - \tau_o m_o, \quad (2)$$

where $S(t, \lambda, m)$ is the signal from the sun-monitoring radiometer at time t , wavelength λ , and representative relative air mass m ; and $S_0(\lambda)$ is the sun signal at the top of the atmosphere when the earth is at distance $D(t)$ equal to 1 AU from the sun. The relative air masses for molecules (m_m), ozone (m_o), and aerosol (m_a) are dependent on the direct irradiance path through the atmosphere (Forgan 1988). In principle, knowledge of the time and location of an observation, together with the atmospheric pressure, allows these terms to be estimated and τ_a determined. While the principle of the measurement is simple, to measure the relatively low magnitude of optical extinction and τ_a in Australia means that the 95% uncertainty has to be less than 0.01 and hence $S_0(\lambda)$ well within 1%.

Calibration of the SPO1A and MFRSR [i.e., determination of an appropriate $\ln S_0(\lambda)$ for each day of the record] was carried out via a multistep process. First, the data were filtered to eliminate water/ice cloud extinction and periods when the optical surfaces were being cleaned (typically just after dawn). Second, the data were analyzed to produce morning and afternoon estimates of $\ln S_0(\lambda)$ using a variety of methods based on Eq. (2). Third, the time series of these estimates were examined to determine the most stable channel over the period of interest using the methods of Forgan (1994). Fourth, the general method (Forgan 1994) using the stable channel as a reference was used to derive better estimates of the time series of $\ln S_0(\lambda)$ for the nonreference wavelengths. Last, these data were averaged for each month, and the resulting statistics were used to represent the monthly mean $\ln S_0(\lambda)$ for each wavelength. These monthly mean data were then used to process the data into transmissions.

All the processing described below was conducted

after the removal of the zero offsets for the SPO1A, and cosine correction and direct irradiance signal derivation for the MFRSR.

The first stage of the calibration process was the application of a set of nine quantitative filters. The filters most active in flagging data as inappropriate for calibration use were as follows.

- 1) The irradiance signals had to be 20 times greater than the uncertainty in the irradiance signal;
- 2) the apparent solar zenith angle had to lie between 0 and 81 (roughly equivalent to air masses 1 through 6); and
- 3) the standard deviations of the active sensor signal during the minutes both before and after an observation had to be less than 0.25% of the estimated active sensor signal at the top of the atmosphere.

The remaining filters flagged periods when the signals were much less than surrounding signals, provided those deviations were greater than twice the 95% uncertainty of the signal measurement. These filters provide similar data flagging to the objective methods of Harrison et al. (1994) but do not remove as many points.

The second stage processing was started by dividing the data remaining each day from the first stage into morning and afternoon periods. From each of these periods data were selected for the time between $m_a = 6$ and the next 90 min closer to solar noon. Provided that more than 30 valid measurements remained in the period, and the range of air mass was 2 or greater, least squares regression (LSR) analyses were performed using modified forms of Eq. (2) as the regression model, namely:

$$\ln S(t, \lambda, m) + \tau_m m_m + \tau_o m_o = [\langle \ln S_0 \rangle_1 - 2 \ln D(t)] - \langle \tau_a \rangle_1 m_a \quad \text{and} \quad (3)$$

$$- [\ln S(t, \lambda, m) + \tau_m m_m + \tau_o m_o] / m_a = \langle \tau_a \rangle_2 - [\langle \ln S_0(\lambda) \rangle_2 - 2 \ln D(t)] / m_a. \quad (4)$$

Both are solved for $\langle \ln S_0(\lambda) \rangle_i$ and $\langle \tau_a \rangle_i$. Equation (3) is a common modified form of the Lambert–Beer–Bouguer law and Eq. (4) is an adaptation of a commonly used technique in astronomy (Young 1974). Both these applications of the LSR reduce the impact of poor representative air mass selection (Forgan 1988) by minimizing the influence of the molecular and ozone extinction components. The resulting data were then used for further analysis if the two estimates $\langle \ln S_0(\lambda) \rangle_1$ and $\langle \ln S_0(\lambda) \rangle_2$ were within 0.005 of each other and the unbiased estimate of the standard deviation of the fit (ϵ) divided by the square root of the number of valid samples was < 0.001 . The mean of the two estimates of $\langle \ln S_0(\lambda) \rangle$, that is,

$$\langle \ln S_0(\lambda) \rangle = [\langle \ln S_0(\lambda) \rangle_1 + \langle \ln S_0(\lambda) \rangle_2] / 2, \quad (5)$$

was obtained.

In the third stage the first estimated calibration series

for each wavelength for any day was based on a zeroth- or first-order polynomial LSR of all the accepted values over the sequence of days (and years) bounded by significant changes in calibration, normally due to instrument alterations. The slope and standard deviation of these estimates were then used to determine the most stable wavelength in the set of wavelengths for the instrument.

For Alice Springs, the most stable wavelength for the SPO1A was the 500-nm channel and the 778-nm channel for the MFRSR. These data were then generated into monthly means and provided there were more than eight good values in each month the mean value was used as the reference for a particular month. If some months had insufficient data, then (provided there were no instrumental changes in the period) monthly mean estimates were interpolated from the nearest acceptable mean value.

The good stability of the calibration in the SPO1A over a period of months [i.e., differences in $\ln S_0(\lambda)$ of less than 0.003] means that use of monthly means did not cause a significant increase in the uncertainty in the transmission. The resulting table of monthly means for the reference wavelength is then used in the next phase of the process. The reference channel is then deemed calibrated and all the filtered data are reanalyzed using the general method (Forgan 1994). The resulting estimates are then filtered iteratively for outliers and $\epsilon > 0.003$. These remaining data are then averaged over each calendar month of the record and the resultant means are used as the calibration values.

In using the above methods, estimates of ozone extinction are required for the analysis of the 500- and 610-nm filter detectors; in this case the annual mean ozone column amount for Brisbane, Australia, was used (Atkinson and Eason 1988). While there would be some improvement on an individual calibration datum if better estimates of the ozone column amount were available (e.g., from Total Ozone Mapping Spectrometer data), the relative improvement on the uncertainty of the calibration (based on the mean value of calibration data) is small.

As a check on the calibrations, one of the other non-reference channel calibrations was used as a substitute reference and the general method analysis repeated. There were no statistically significant differences (at the 95% level) in the original and substitute reference calibrations.

A detailed uncertainty analysis based on the ISO Guide to the Uncertainty of Measurement (ISO 1995) was performed on the measurement system and the subsequent derivation of aerosol optical depth for any time (t). The analysis suggests that, using a consistent model for molecular and ozone extinction, and a calibration value estimated from at least 30 equivalent samples, the U_{95} (95% confidence interval) in aerosol optical depth for all four SPO1A wavelengths was less than 0.010. A uncertainty analysis for the MFRSR gave similar results

provided the directional response of the detector was known to within 0.1%.

2) CE318

Calibration of direct sun measurements of the CE318 sun photometer was performed using a combination of modified Langley regression and the general method (Forgan 1994). The adopted form of the modified regression equation [similar to Eq. (4)] was

$$\frac{1}{m} \ln S(t, \lambda, m) = \frac{1}{m} [\langle \ln S_0(\lambda) \rangle - 2 \ln D(t) - \langle \tau(\lambda) \rangle], \quad (6)$$

where the unsubscripted air mass m and total optical depth τ are defined as

$$m = (\tau_m m_m + \tau_a m_a + \tau_o m_o) / \tau \quad (7)$$

$$\tau = \tau_m + \tau_a + \tau_o. \quad (8)$$

Equation (6) was solved for the estimates $\langle \ln S_0(\lambda) \rangle$ and $\langle \tau(\lambda) \rangle$ over observation periods defined according to the following criteria. First, only observations obtained between air masses 2 and 6 were included. Second, for each direct sun acquisition, the CE318 makes three distinct measurements spaced 30 s apart. The coefficient of variation (CV) amongst this ‘‘triplet’’ provides a useful indication of atmospheric stability, noisy triplets often indicating the presence of clouds. Based on experience and with reference to Smirnov et al. (2000), triplets with $CV > 1\%$ were rejected. Following this step, the number of triplets remaining in each of the four unit airmass intervals (2–3, 3–4, 4–5, and 5–6) was examined. If there were fewer than two triplets remaining in each interval, Langley analysis of the measurement set was abandoned. Finally, any candidate regression period was rejected if $\epsilon > 0.005$.

In practice, calibration of the CE318 data at Alice Springs was performed as follows.

- The Langley method as described above was applied to all data during the study period.
- Drift due to filter ageing was accommodated by fitting a linear trend to the time series of $\ln S_0$ in each channel.
- A reference channel was selected based on the smallest rms deviation about this linear trend; in the present case the 870-nm channel fulfilled this criterion.
- The general method was applied using the 870-nm channel as reference, and a new set of linear trends in $\ln S_0$ was found.
- Rms deviations about these trends allowed identification of the 778-nm channel as a second reference channel.
- The general method was reapplied using the 778-nm channel as reference.
- The general method was reapplied using the 500-nm channel as reference.

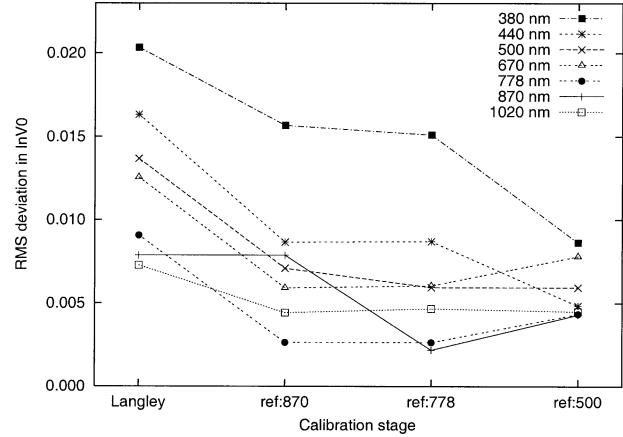


FIG. 2. Change in rms deviation of $\ln S_0$ following successive applications of the general method using different reference channels.

The improvement in calibration accuracy following this method is illustrated in Fig. 2. The general method allows reduction of the rms error in $\ln S_0$ by better than a factor of 2 at all wavelengths except 1020 nm. Also, it is evident that the general method is most effective for channels spectrally similar to the reference channel, where departures from the assumption of a stable aerosol size distribution inherent in the method have less impact. The figure also shows that there is little improvement in the variance of the CE318 channels if multiple, non-independent, reference wavelengths are used. The exceptions are the 380- and 440-nm channels that are spectrally distant in extinction from the initial reference at 870 nm. The adopted set of linear trends in $\ln S_0$ was based on the general method result with smallest rms deviation, as shown in Table 1.

The calibration of the two CE318 photometers at Tinga Tingana was modified slightly to accommodate the different bandpass filter configuration of these instruments. The general method was applied twice, first using 870 nm as the reference channel, then repeated using 670 nm. Standard deviations in $\ln S_0$ derived for these photometers and shown in Table 1 were comparable to that obtained at Alice Springs, except that the 440-nm result was somewhat more noisy owing to the lack of a 500-nm channel on the Tinga Tingana instruments.

3. Observations

The CE318 was installed at the Bureau of Meteorology meteorological observing station at Alice Springs (23°47'52''S, 133°53'17''E) on 13 February 2000, at which time both the SPO1A and MFRSR had been in operation for extended periods. The three-way comparison was brief, ending on 22 March 2000 with the failure and removal of the MFRSR. The comparison between the SPO1A and CE318 continued until 5 May 2000 when problems with the SPO1A solar tracking device caused termination. The CE318 was serviced on 11 June

Table 1. Adopted reference channels and std devs in calibration coefficient $\ln S_0$ for the CE318 sun photometers.

Channel (nm)	Alice Springs: no. 4		Tinga Tingana: no. 2		Tinga Tingana: no. 3	
	Reference (nm)	σ ($\ln S_0$)	Reference (nm)	σ ($\ln S_0$)	Reference (nm)	σ ($\ln S_0$)
380	500	0.0086				
440	500	0.0048	670	0.0073	670	0.0069
500	778	0.0059				
670	870	0.0059	870	0.0033	870	0.0030
778	870	0.0026				
870	778	0.0022	670	0.0026	670	0.0026
1020	870	0.0044	670	0.0043	670	0.0062

2000 and removed from Alice Springs on 15 September 2000 for deployment elsewhere. Hence the comparison between the SPO1A and CE318 covers the period 13 February–5 May 2000.

The two CE318 instruments were installed at Tinga Tingana (28°58'33"S, 139°59'27"E) on 1 April 1998. The site was serviced on 1 July 1998 to address satellite phone problems. The comparison concluded on 16 July 1998 following a power supply failure.

Data screening

Data included in the comparison were drawn only from days on which at least one Langley period (either a.m. or p.m. or both) was found following the selection criteria given in section 2c2 above. Within these days, the CE318 data were further screened. Tests included those already described to select points for Langley analysis, and a further test involving formation of a daily mean and standard deviation, followed by rejection of any measurements where the aerosol optical depth is more than 3 standard deviations from the mean. This test was applied iteratively until all measurements passed.

Selection of intercomparison data within each day was carried out by comparing acquisition times of the SPO1A and MFRSR with those from the fully screened

CE318 data. A valid match was declared when the time stamps differed by less than 30 s, half the sampling interval of the SPO1A. For the CE318–SPO1A comparison period of 83 days, this left 28 days with a total of 4094 matchups of instantaneous atmospheric transmission. For the three-way comparison period of 39 days, there were 9 days and a total of 1436 matchups.

For the Tinga Tingana comparison, a valid match was declared when the time stamps differed by less than 15 s, half the interval between triplet observations on the CE318. In this comparison period of 107 days, 39 days passed the screening criteria, leading to a total of 5258 matchups.

4. Results

a. CE318–SPO1A

There are two coincident bandpass filters on this pair of instruments, with nominal effective wavelengths of 500(500.2) nm and 870(868) nm for the CE318 (SPO1A). Figure 3 shows the total optical depth difference at 500 nm between the two instruments as a function of air mass. The corresponding comparison at 868 nm is shown in Fig. 4. The total optical depth was derived from the transmission via

$$\tau(\lambda) = \ln T(\lambda)/m. \quad (9)$$

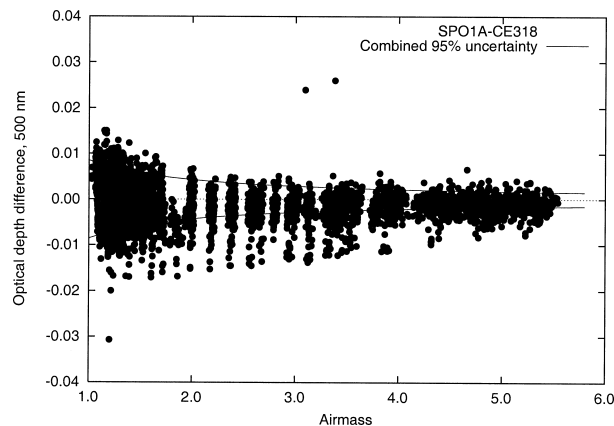


FIG. 3. Differences in optical depth at 500 nm between SPO1A and CE318, plotted as a function of air mass. The solid lines indicate the 95% uncertainty interval based on an uncertainty analysis for each instrument.

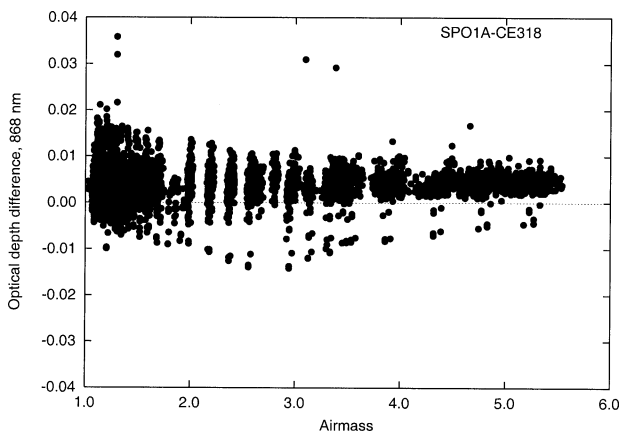


FIG. 4. Differences in optical depth at 868 nm between SPO1A and CE318, plotted as a function of air mass.

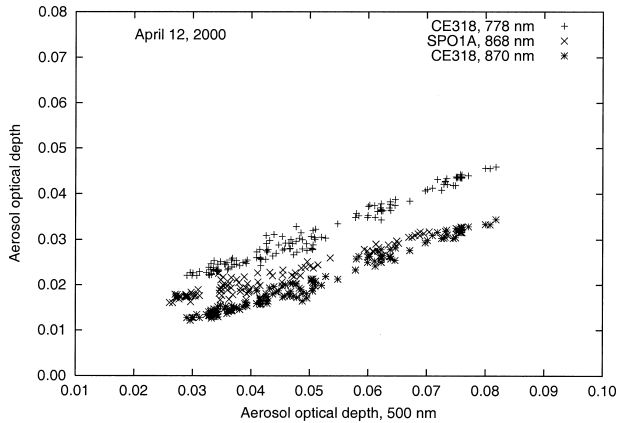


FIG. 5. Comparison of interchannel variation of aerosol optical depth during 12 Apr 2000. The aerosol optical depth at 868 nm recorded by the SPO1A lies between the 778- and 870-nm aerosol optical depth recorded by the CE318.

The use of total optical depth rather than aerosol optical depth as a measurand avoids systematic errors that may arise from different assumptions regarding Rayleigh scattering and ozone amount.

At 500 nm, Fig. 3 shows differences symmetrically scattered about zero bounded by an envelope whose amplitude diminishes with air mass. The origin of this can be seen in a simplified analysis considering standard uncertainty (ISO 1995) in optical depth $u(\tau)$ consequent only on uncertainties $u(S)$ in signal and $u(S_0)$ in calibration value. In this case,

$$u(\tau) = \left(\left[\frac{u(S)}{mS} \right]^2 + \left[\frac{u(S_0)}{mS_0} \right]^2 \right)^{1/2}. \quad (10)$$

Hence, component uncertainties in the signal $u(S)$ will appear as an optical depth uncertainty $u(\tau)$ that decays with air mass m , until an inflection point at $m = \tau^{-1}$, after which the uncertainty will start to increase with increasing m . The calibration term decreases linearly with air mass. For conditions in central Australia, $u(\tau)$ produces a deviation that decays with air mass until $m > 6$ for wavelengths > 500 nm. This is well represented in Fig. 3, suggesting that neither calibration bias nor signal precision contributes significantly to the difference between these two systems at 500 nm.

A comprehensive uncertainty analysis has been carried out for both systems, considering contributions from digitization noise, calibration, dark count, nonlinearity, time variation of window transmission, and air mass. As an example, the solid line in Fig. 3 shows the combined 95% uncertainty of the differences in total optical depth of the SPO1A and CE318 as a function of air mass. The dominant source of uncertainty arises from nonlinearity and variable window transmission.

Figure 4 shows the corresponding scatterplot at 868 nm. Unlike the symmetrical scatter about zero difference seen at 500 nm, this diagram shows a clear positive bias independent of air mass. This is not a calibration error,

Table 2. Ensemble bias and std dev of the difference between the optical depths measured by the SPO1A and CE318 photometers.

SPO1A–CE318 (no. 4)			
28 days, 4094 matchups			
λ_{SPO1A}	λ_{CE318}	Bias	σ
500.2	500	−0.0014	0.0047
868.0	870	0.0039	0.0039

which, following Eq. (10), would introduce an m^{-1} dependence in the shape of the envelope. The constant offset in optical depth suggests an offset in the spectral bandpasses of the two instruments, with sufficiently stable Ångström coefficient from day to day produce a clear net bias.

This explanation is confirmed in Fig. 5, which shows interchannel aerosol optical depth for the two photometers on 12 April 2000. The locus of variation in SPO1A aerosol optical depth at 868 nm lies between those recorded by the CE318 at 778 and 870 nm. Further confirmation was provided by inspection of the station and calibration record of the SPO1A 868-nm channel, which showed a shift in calibration following maintenance work carried out during January 1999. The bias is likely due to filter degradation in the form of sideband leakage caused by moisture ingress.

Table 2 lists mean bias and standard deviation σ for the total optical depth differences shown in Figs. 3 and 4. The diagnosis of spectral leakage at 868 nm manifests statistically as a bias equal to the standard deviation (0.0039), in contrast to the situation at 500 nm where the bias (−0.0014) is less than one-third of the standard deviation.

b. CE318–MFRSR

The six-channel MFRSR has an 867-nm filter coincident with the SPO1A 868-nm and CE318 870-nm bandpasses, and a further two at 672 and 777 nm coincident with the 670- and 778-nm channels on the CE318. A scatterplot of the optical depth differences between the MFRSR and CE318 at 672 nm is shown in Fig. 6; plots at the two longer wavelengths are similar. The scatterplots show strong air mass dependence with large positive errors at low air mass. This leads to large bias errors, shown in Table 3 to lie between 0.013 and 0.014, with standard deviations above 0.01 in all channels.

Figure 7 illustrates the origin of the large bias and standard deviation of the MFRSR–CE318 optical depth difference, by revealing a large diurnal variation in the 865-nm difference of order 0.02. By contrast, the SPO1A–CE318 difference is of order 0.005 and has the opposite shape. The diurnal effect in the MFRSR signal was seen in the intercomparison of four radiometers during the ARM intensive observation period during 1997 (Schmid et al. 1999). The effect is also discussed on the ARM World Wide Web site (<http://www.arm.gov/>)

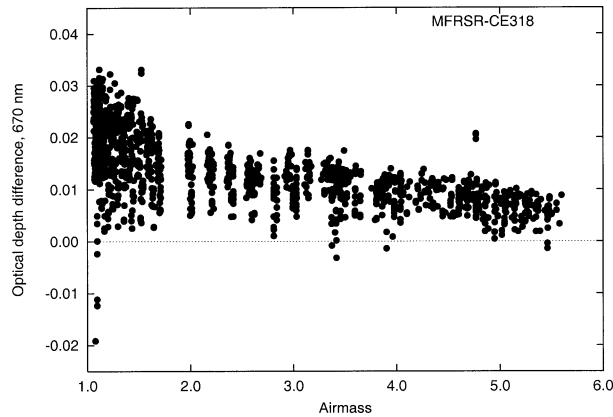


FIG. 6. Differences in optical depth at 670 nm between the MFRSR and CE318 photometers, plotted as a function of air mass.

docs/instruments/static/mfrsr.html) and attributed to temperature sensitivity, even though the instrument cavity is temperature stabilized.

In the present case, Fig. 7 shows that the MFRSR–CE318 optical depth difference is markedly asymmetric about local solar noon. In addition, the peak difference occurs significantly before noon. This behavior suggests a combination of misalignment and incorrect cosine response characterization. Misalignment of the sensor plane relative to the instrument housing may be a factor, despite use of a leveling procedure designed to avoid this. Further evidence for error in response characterization arises from an examination of the derived S_0 values, which indicate a bias between afternoon and morning monthly mean values with a separation of approximately 2%. Clearly, careful attention to sensor plane alignment and cosine response characterization is essential to ensure the quality of data from this instrument.

c. CE318(2)–CE318(3)

Optical depth differences between the two CE318 photometers operated at Tinga Tingana during 1998 are shown in Fig. 8 for the 440-nm channel, plots at other wavelengths being similar. These plots show tight correlations with symmetry about zero difference. The daily and ensemble mean bias and rms deviations are shown in Table 4. The ensemble mean biases are negligible, the largest being -0.0004 at 870 nm; standard

Table 3. Ensemble bias and std dev of the difference between the optical depths measured by the MFRSR and CE318 photometers.

MFRSR–CE318 (no. 4) 9 days, 1436 matchups			
λ_{MFRSR}	λ_{CE318}	Bias	σ
672	670	0.0137	0.0104
777	778	0.0128	0.0120
867	870	0.0125	0.0114

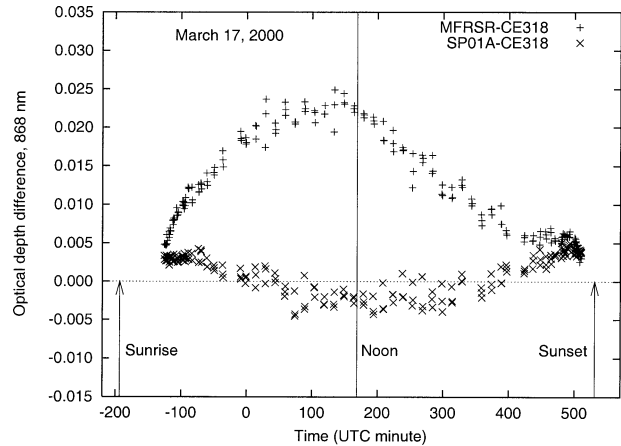


FIG. 7. Differences in optical depth at 868 nm as a function of time during 17 Mar 2000. The vertical lines indicate the times of sunrise, local solar noon, and sunset.

deviations vary between 0.0013 at 670 nm and 0.0025 at 870 nm. Since the instruments and signal processing systems are identical, these values are interpreted as a measure of instrumental repeatability or precision.

5. Discussion

In a comparable study, Schmid et al. (1999) compared aerosol optical depths derived from four radiometers at the ARM site in Oklahoma over a 15-day period in 1997. The instruments included a Cimel CE318, a MFRSR, the Ames Airborne Tracking Sunphotometer (AATS6), and a rotating shadowband spectroradiometer (RSS). The AATS6 was chosen as the reference instrument, so the difference sets relevant to the present work are CE318–AATS6 and MFRSR–AATS6.

Figure 9 shows the standard deviation of the difference in optical depth plotted as a function of bias in the difference. There is a clear demarcation between the sets SPO1A–CE318 and CE318(nos. 3–2), where both

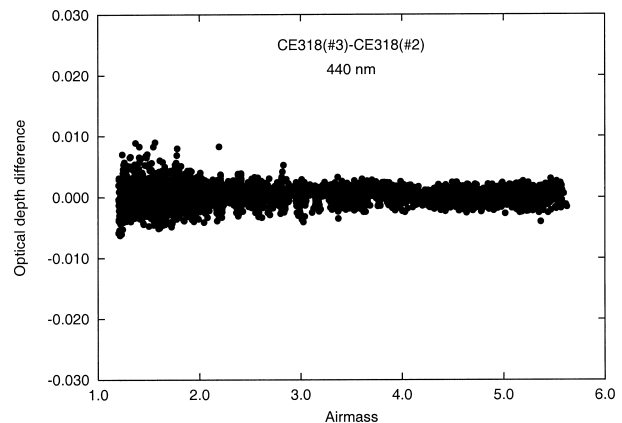


FIG. 8. Differences in optical depth at 440 nm between the two CE318 photometers(nos. 3–2), plotted as a function of air mass.

Table 4. Ensemble bias and std dev of the difference between the optical depths measured by two CE318 photometers (nos. 3–2).

CE318 (nos.3–2) 39 days, 5258 matchups		
λ	Bias	σ
440	0.0002	0.0015
670	-0.0001	0.0013
870	-0.0004	0.0025
1020	-0.0001	0.0020

bias and standard deviation are within ± 0.005 , and the remaining results. For both comparisons involving the MFRSR, the standard deviations are comparable, in the range 0.010–0.013, while the biases are very different. This suggests that the effect leading to the bias of ≈ 0.013 in the present study is related to the particular instrument and quality of the angular response characterization, but that the random component is generic.

The results from Schmid et al. for the CE318–AATS6 differences straddle a wide range in bias and standard deviation intermediate between the other sets, suggesting a combination of errors from calibration (leading to the bias) and random measurement error. It should be pointed out that the differences reported by Schmid et al. are for aerosol optical depth, not total optical depth as in the present study, so that systematic errors may arise due to differences in assumed Rayleigh scattering

and ozone corrections. However, estimates of these effects show them to be small in the present context (Schmid et al. 1999).

Combined uncertainty limits are imposed by the random components of the instrumental differences, not any bias, which in principle (ISO 1995) should be removed. However, if biases cannot be removed they must be included in estimated uncertainties (ISO 1995). Accordingly, Fig. 10 shows the 95% uncertainty in optical depth, $U_{95} = 2\sigma$, based on the standard deviation σ from the present difference sets and also those listed by Schmid et al. (1999) assuming biases have been removed. Examination of Fig. 10 yields the following conclusions.

- 1) The precision of the CE318 measurement of total optical depth lies below 0.005 at all wavelengths.
- 2) The 95% uncertainty implied by the SPO1A–CE318 difference lies below 0.01 at both comparison wavelengths. If this difference is divided equally between the two instruments (as suggested by the precision level of the CE318), then the 95% uncertainty associated with each instrument is < 0.007 under Australian conditions.
- 3) As noted above, the uncertainties associated with the MFRSR are comparable in both the present study and that of Schmid et al. (1999). Figure 10 suggests that the 95% uncertainty of the MFRSR lies in the range 0.020–0.025.

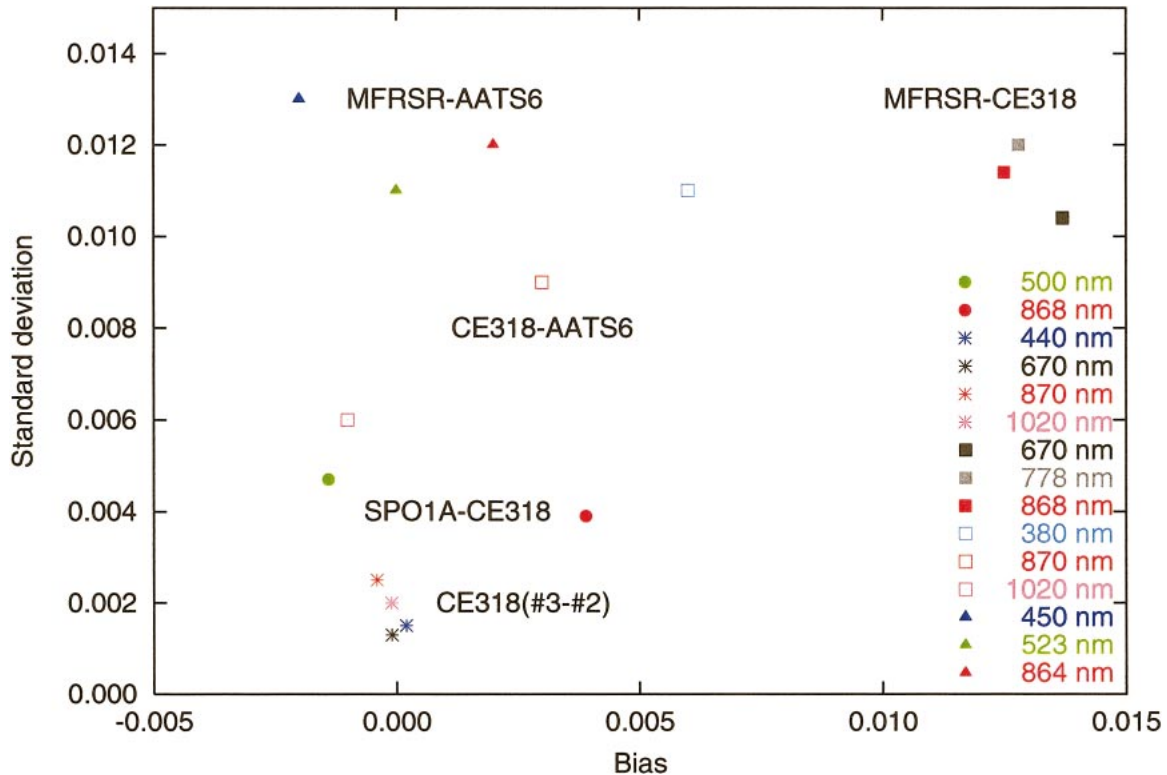


FIG. 9. Std dev of ensemble differences in optical depth plotted against ensemble bias. As well the three difference sets reported in the present study, two additional sets from Schmid et al. (1999) are included (see text).

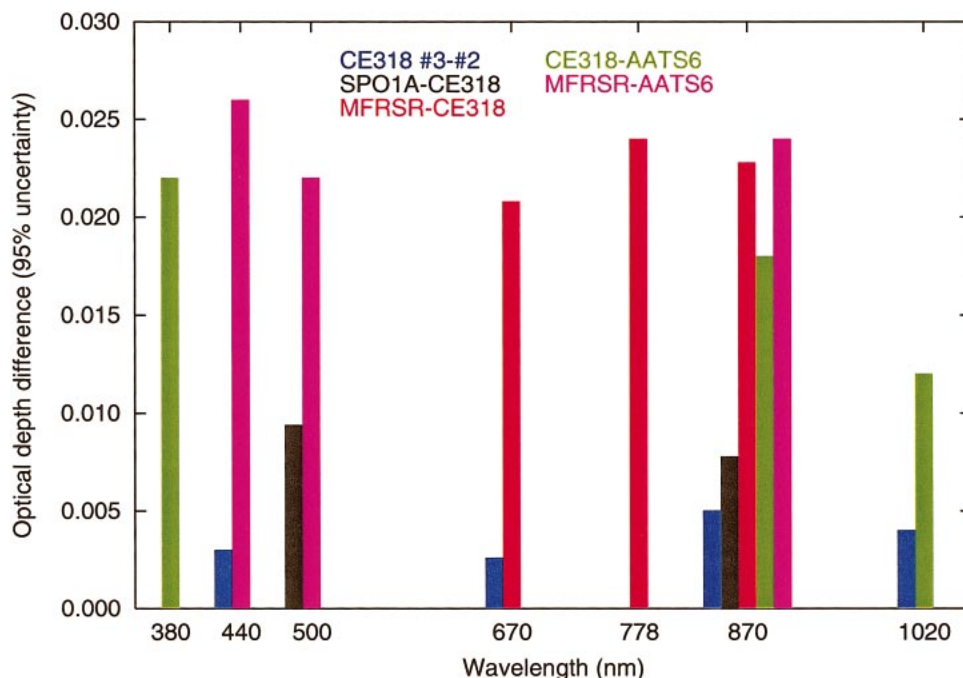


FIG. 10. 95% uncertainties derived from the std dev of ensemble differences in optical depth. The three difference sets reported in the present study are shown as blue, black, and red bars while the two additional sets from Schmid et al. (1999) are shown in green and magenta.

- 4) The 95% uncertainty implied by the CE318–AATS6 differences reported by Schmid et al. falls in the range 0.012–0.022, over a factor of 2 higher than the intrinsic uncertainty of the CE318 inferred above. This suggests either a substantial uncertainty contribution from the AATS6 or, more likely, a greater random error due to the different aerosol regime and shorter comparison period covered by the Schmid et al. study. In any case, it appears reasonable to conclude that collimated instruments such as the CE318 and SPO1A are capable of resolving total optical depth to better than 0.007 when calibrated at sea level remote inland Australian sites, about a factor of 2 better than is achieved by comparable instruments operated in the Northern Hemisphere, using calibrations obtained at high altitude sites.

6. Uncertainty in CE318 aerosol optical depth

Since aerosol optical depth is derived from total optical depth by subtracting the optical depths due to Rayleigh scattering and ozone absorption, uncertainties in these must be included when deriving the uncertainty in aerosol optical depth. Uncertainty in the Rayleigh scattering optical depth arises from inexact knowledge of the surface pressure p , while that for ozone relates to uncertainty in the column ozone amount q . Following ISO (1995), if the standard uncertainties in p and q are $u(p)$ and $u(q)$, respectively, then the combined uncertainty in aerosol optical depth is

$$u(\tau_a) = \{u^2(\tau) + [c_p u(p)]^2 + [c_q u(q)]^2\}^{1/2}, \quad (11)$$

where $u(\tau)$ is the standard uncertainty in total optical depth, c_p is the molecular extinction sensitivity factor for $u(p)$, and c_q is the ozone extinction sensitivity factor for $u(q)$.

Secondary contributions to aerosol optical depth uncertainty not included in this analysis arise from uncertainty in air mass and from absorption by NO_2 , the latter mainly in the blue spectral region. As discussed above, individual species air masses based on typical distributions of aerosol, ozone, and molecules were used (Forgan 1988). Since there was no evidence of significant high altitude (>8 km) aerosol during the comparisons, the contribution to the air mass uncertainty of highly distorted vertical distributions of constituents was not included in the analysis. However, if species air masses were neglected and the classical Langley method used, the uncertainty must include the impact of calibration biases of $\sim 1\%$.

The NO_2 column amounts above the remote locations used in this study are dominated by stratospheric concentrations and are typically $\sim 3 \times 10^{-15}$ molecules cm^{-2} . Based on published absorption coefficients (e.g., Burrows et al. 1998), NO_2 absorption would increase the optical depth by < 0.002 at 380 and 440 nm and by < 0.001 at 500 nm. Near-real-time global distributions of NO_2 from the Global Ozone Monitoring Experiment (Loyola and Erbertseder 2001) offer a means of correcting derived aerosol optical depths for this absorber.

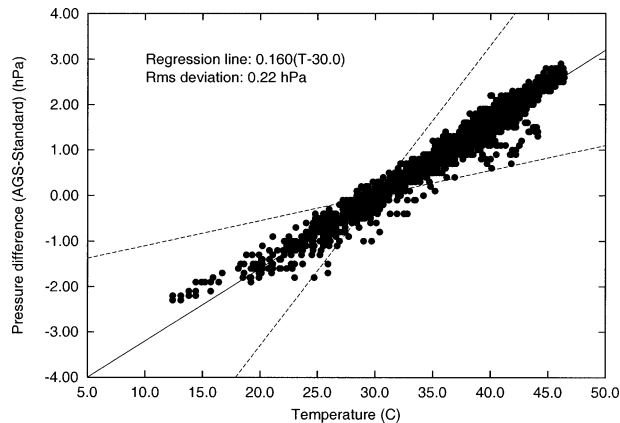


FIG. 11. Error in barometric pressure determined from the SensorTechnics barometer used in the AGSNet system as a function of enclosure temperature. The dashed lines indicate the range of temperature coefficients specified by the sensor manufacturer.

a. Surface pressure

Surface pressure at AGSNet stations is measured using an electronic barometer manufactured by SensorTechnics. The location of an AGSNet system at a Bureau of Meteorology station provided an opportunity to assess the performance of this instrument. Before deployment, the SensorTechnics units are calibrated against a standard aneroid barometer, that is in turn regularly calibrated against a Bureau of Meteorology standard. Ten-minute mean AGSNet pressures at Alice Springs were compared to corresponding means measured at the meteorological station. This comparison revealed a small error that depends linearly on the operating temperature of the AGSNet barometer, as shown in Fig. 11. Statistical analysis of these errors shows a bias of 0.87 hPa and a standard deviation of 1.1 hPa over the entire comparison period. The resulting standard uncertainty in pressure in this case is $u(p) = [(1.1)^2 + (0.87/\sqrt{3})^2]^{1/2} = 1.4$ hPa, where the factor of $\sqrt{3}$ arises from the assignment of a rectangular function to the distribution of the bias error. A least squares regression of the data shown in Fig. 11 allows temperature compensation with a standard uncertainty of 0.22 hPa based on the rms deviation of the fit.

Surface pressure is not measured at standard AERONET sites, which rely on climatology for pressure estimates. Statistical analysis of pressure data from Tinga Tingana over the year 2000 yields an annual mean of 1011 hPa with a standard deviation of 6.5 hPa. Inspection of the histogram shows significant departures from a normal distribution, with the variation more conservatively represented by a rectangular function with semirange 14 hPa, leading to a standard uncertainty of 8.1 hPa.

b. Ozone amount

Correction for ozone at AGSNet sites is performed using monthly mean ozone amounts measured at BoM

Table 5. Increase in 95% uncertainty in aerosol optical depth over that for total optical depth [$U_{95}(\tau) = 0.007$] arising from uncertainty in surface pressure and ozone amount. The three columns correspond to standard uncertainties in surface pressure of 8.1 hPa (climatology), 1.4 hPa (uncompensated SensorTechnics barometer), and 0.22 hPa (compensated SensorTechnics barometer). The standard uncertainty in ozone amount was 0.023 atm-cm.

Channel (nm)	$u(p) = 8.1$ hPa	$u(p) = 1.4$ hPa	$u(p) = 0.22$ hPa
380	0.0030	0.0001	0.0000
440	0.0010	0.0000	0.0000
500	0.0005	0.0002	0.0002
670	0.0004	0.0003	0.0003
778	0.0000	0.0000	0.0000
870	0.0000	0.0000	0.0000
1020	0.0000	0.0000	0.0000

stations located at commensurate latitudes. For example, data from Tinga Tingana (28°59'S) are corrected using ozone measured at Brisbane (27°28'S). Statistical analysis of four years' daily ozone data from Brisbane yields monthly means ranging from 0.256 to 0.311 atm-cm with monthly semiranges between 0.011 and 0.039 atm-cm. Hence a conservative estimate of the standard uncertainty is obtained by choosing $u(q) = 0.039/\sqrt{3} = 0.023$ atm-cm.

The impact of these component uncertainties is summarized in Table 5, which shows the incremental increase in uncertainty ΔU_{95} defined as

$$\Delta U_{95} = U_{95}(\tau_a) - U_{95}(\tau), \tag{12}$$

where a coverage factor of 2 is assumed throughout so that $U_{95}(x) = 2u(x)$. Hence, $u(\tau) = 0.0035$ since $U_{95}(\tau)$ was found to be ≤ 0.007 in a previous section.

Table 5 shows uncertainty increments for three values of $u(p)$ corresponding to climatology (8.1 hPa), uncompensated in situ barometer (1.4 hPa), and compensated in situ barometer (0.22 hPa). The only significant increase in uncertainty is found for climatological pressure at 380 nm, where $U_{95}(\tau_a)$ is boosted by 0.003 over $U_{95}(\tau)$ to 0.010. In all other cases the increase is at or below 0.001 and therefore insignificant. The maximum effect of ozone is seen at 670 nm but only at the 0.0003 level. The use of the SensorTechnics barometer without temperature compensation clearly provides more than an adequate pressure determination with negligible uncertainty increments at all wavelengths examined here.

7. Conclusions

Intercomparison of sun photometers at sites in the Australian outback has demonstrated agreement between the Carter–Scott SPO1A used in the BoM network and the Cimel CE318 used at CSIRO stations to better than 0.01 at the 95% level, suggesting that each is capable of measuring total optical depth to better than 0.007. This result was obtained using independent hardware and processing software, and in situ calibration. The accuracy demonstrated meets the requirements of

the BSRN to provide aerosol optical depth to 0.01 or better at the 95% uncertainty level. A third instrument included in the study, the MFRSR, showed $U_{05} > 0.02$, a result confirmed by a comparable study in the Northern Hemisphere. This suggests that this instrument is unsuitable for aerosol optical depth measurement under Australian conditions, where background levels are typically ≈ 0.02 in the midvisible.

The impact of uncertainties in surface pressure and ozone on the uncertainty in aerosol optical depth is shown to be negligible given in situ pressure measurement to 1.4 hPa and monthly mean ozone data from stations at commensurate latitude to the observing site. These results will underpin the joint development of aerosol climatologies based on data from both BoM and CSIRO stations across the Australian continent.

Acknowledgments. The authors wish to thank Drs. D. M. O'Brien and R. D. Graetz for stimulating discussions and generous assistance with field work. Support from the electronic and mechanical workshops at CSIRO Atmospheric Research is gratefully acknowledged. Nels Larsen kindly provided direct access to the MFRSR at Alice Springs.

REFERENCES

- Atkinson, R. J., and J. R. Eason, 1988: Reevaluation of the Australian Total Column Ozone Data Record. *Ozone in the Atmosphere: Proceedings of the Quadrennial Ozone Symposium 1998 and Tropospheric Ozone Workshop*, A. Deepak, 168–171.
- Burrows, J. P., A. Dehn, B. Deters, S. Himmelmann, A. Richter, S. Voigt, and J. Orphal, 1998: Atmospheric remote-sensing reference data from GOME. Part 1: Temperature-dependent absorption cross-sections of NO_2 in the 231–794 nm range. *J. Quant. Spectrosc. Radiat. Transfer*, **60**, 1025–1031.
- Christopher, S. A., X. Li, R. M. Welch, J. S. Reid, P. V. Hobbs, T. F. Eck, and B. N. Holben, 2000: Estimation of surface and top-of-atmosphere shortwave irradiance in biomass-burning regions during SCAR-B. *J. Appl. Meteor.*, **39**, 1742–1752.
- Forgan, B. W., 1988: Comment on: Bias in solar constant determination by the Langley method due to structured atmospheric aerosol. *Appl. Opt.*, **27**, 2546–2548.
- , 1994: General method for calibrating sun photometers. *Appl. Opt.*, **33**, 4841–4850.
- , J. J. DeLuisi, B. B. Hicks, and E. N. Rusina, 1994: Report on the measurements of Atmospheric Turbidity in BAPMoN. WMO Tech. Doc. 603, GAW Rep. 94, 77 pp.
- Gras, J. L., J. B. Jensen, K. Okada, M. Ikegami, Y. Zaizen, and Y. Makino, 1999: Some optical properties of smoke aerosol in Indonesia and tropical Australia. *Geophys. Res. Lett.*, **26**, 1393–1396.
- Harrison, L., J. Michalsky, and J. Berndt, 1994: Automated multifilter rotating shadowband radiometer: An instrument for optical depth and radiation measurements. *Appl. Opt.*, **33**, 5118–5125.
- Holben, B. N., and Coauthors, 1998: AERONET—A federated instrument network and data archive for aerosol characterization. *Remote Sens. Environ.*, **66**, 1–16.
- , and Coauthors, 2001: An emerging ground-based aerosol climatology: Aerosol optical depth from AERONET. *J. Geophys. Res.*, **106**, 12 067–12 097.
- ISO, 1995: Guide to the expression of uncertainty in measurement. International Organization for Standardization, Switzerland, 101 pp.
- Kaufman, Y. J., A. W. Setzer, D. Ward, D. Tanré, B. N. Holben, P. Menzel, M. C. Pereira, and R. Rasmussen, 1992: Biomass burning airborne and spaceborne experiment in the Amazonas (Base-A). *J. Geophys. Res.*, **97**, 14 581–14 599.
- Loyola, D., and T. Erbertseder, cited 2001: Near-real-time global ozone network from GOME (N-GONG): NO_2 . German Aerospace Center (DLR). [Available online at http://auc.dfd.dlr.de/GOME_NRT/no2.html.]
- McTainsh, G. H., and J. R. Pitblado, 1987: Dust storms and related phenomena measured from meteorological records in Australia. *Earth Surf. Processes Landforms*, **12**, 415–424.
- Michalsky, J. J., J. A. Schlemmer, W. E. Berkheiser, J. L. Berndt, and L. C. Harrison, 2001: Multiyear measurements of aerosol optical depth in the Atmospheric Radiation Measurement and Quantitative Links programs. *J. Geophys. Res.*, **106**, 12 099–12 107.
- Ohmura, A., and Coauthors, 1998: Baseline Surface Radiation Network (BSRN/WCRP): New precision radiometry for climate research. *Bull. Amer. Meteor. Soc.*, **79**, 2115–2136.
- Penner, J. E., and Coauthors, 2001: Aerosols, their direct and indirect effects. *Climate Change 2001: The Scientific Basis: Contribution of Working Group I to the Third Assessment Report of the Intergovernmental Panel on Climate Change*, J. T. Houghton et al., Eds., Cambridge University Press, 289–348.
- Rosen, J., S. A. Young, J. Laby, N. Kjöme, and J. L. Gras, 2000: Springtime aerosol layers in the free troposphere over Australia: Mildura Aerosol Tropospheric Experiment (MATE 98). *J. Geophys. Res.*, **105**, 17 833–17 842.
- Rotstayn, L. D., 1999: Indirect forcing by anthropogenic aerosols: A global climate model calculation of the effective-radius and cloud-lifetime effects. *J. Geophys. Res.*, **104**, 9369–9380.
- Russell, P. B., P. V. Hobbs, and L. L. Stowe, 1999: Aerosol properties and radiative effects in the United States East Coast haze plume: An overview of the Tropospheric Forcing Observational Experiment (TARFOX). *J. Geophys. Res.*, **104**, 2213–2222.
- Schmid, B., and Coauthors, 1999: Comparison of aerosol optical depth from four solar radiometers during the fall 1997 ARM intensive observation period. *Geophys. Res. Lett.*, **26**, 2725–2728.
- Scott, W. D., B. W. Forgan, and J. M. Prospero, 1992: Atmospheric turbidity measurements at Broome in Western Australia. *J. Roy. Soc. West. Aust.*, **75**, 111–118.
- Sibson, B., and B. W. Forgan, 1987: CGBAPS active tracker system for equatorial mounts. *Baseline Atmospheric Program (Australia) 1985*, B. W. Forgan and P. J. Fraser, Eds., Melbourne Bureau of Meteorology in cooperation with CSIRO Division of Atmospheric Research, 38–41.
- Smirnov, A., B. N. Holben, T. Eck, O. Dubovik, and I. Slutsker, 2000: Cloud-screening and quality control algorithms for the AERONET database. *Remote Sens. Environ.*, **73**, 337–349.
- Tegen, I., and I. Fung, 1994: Modeling of mineral dust in the atmosphere: Sources, transport, and optical thickness. *J. Geophys. Res.*, **99**, 22 897–22 914.
- , A. A. Lacis, and I. Fung, 1996: The influence on climate forcing of mineral aerosols from disturbed soils. *Nature*, **380**, 419–422.
- Ward, D. E., and Coauthors, 1992: Smoke and fire characteristics for cerrado and deforestation burns in Brazil: Base-B experiment. *J. Geophys. Res.*, **97**, 14 601–14 619.
- WMO, 2001: Report on sixth BSRN science and review workshop, Melbourne, Australia, May 2000. WCRP Rep. 17/2001, 29 pp.
- Young, A. T., 1974: Observational technique and data reduction. *Methods Exp. Phys.*, **12**, 123–192.